International Journal of Bifurcation and Chaos, Vol. 27, No. 9 (2017) 1750137 (16 pages)
© World Scientific Publishing Company
DOI: 10.1142/S0218127417501371

Int. J. Bifurcation Chaos 2017.27. Downloaded from www.worldscientific.com
by HONG KONG POLYTECHNIC UNIVERSITY on 04/20/19. Re-use and distribution is strictly not permitted, except for Open Access articles.

Noise-Induced Chaos in a Piecewise Linear System

Chen Kong* and Xian-Bin Liu†
State Key Laboratory of Mechanics and Control of Mechanical Structures,
Nanjing University of Aeronautics and Astronautics,
29 Yudao Street, Nanjing, Jiangsu Province, P. R. China
**kongchen_bill@126.com*
†*xbliu@nuaa.edu.cn*

Received December 15, 2016; Revised April 18, 2017

In the present paper, the phenomenon of noise-induced chaos in a piecewise linear system that is excited by Gaussian white noise is investigated. Firstly, the global dynamical behaviors of the deterministic piecewise linear system are investigated numerically in advance by using the generalized cell-mapping digraph (GCMD) method. Then, based on these global properties, the system that is excited by Gaussian white noise is introduced. Then, it is simplified by the stochastic averaging method, through which, a four-dimensional averaged Itô system is finally obtained. In order to reveal the phenomenon of noise-induced chaos quantitatively, MFPT (the mean first-passage time) is selected as the measure. The expression for MFPT is formulated by using the singular perturbation method and then a rather simple representation is obtained via the Laplace approximation, and within which, the concept of quasi-potential is introduced. Furthermore, with the rays method, the MFPT under a certain set of parameters is estimated. However, within the process of analysis, the authors had to face a difficult problem concerning the ill-conditioned matrix, which is the obstacle for the estimation of MFPT, which was then solved by applying one more approximation. Finally, the result is compared with the numerical one that is obtained by the Monte Carlo simulation.

Keywords: Piecewise linear system; intermittent switching behavior; noise-induced chaos; MFPT.

1. Introduction

In recent years, there has been considerable interest in the research on the phenomena of noise-induced dynamical behaviors in the field of random dynamical systems. Thus far, many of these phenomena, such as, the so-called noise-induced chaos [He & Habib, 2013; Tél *et al.*, 2008; Lin & Young, 2008], intermittent switching behavior [Armbruster *et al.*, 2003; Stone & Armbruster, 1999], noise-induced switching between cycles in the heteroclinic networks [Armbruster *et al.*, 2003; Stone & Armbruster, 1999], synchronization [Zhou *et al.*, 2003], a lowering of the escape energy [Kraut & Feudel, 2003a; Hunt *et al.*, 1996], transient chaos [Tél *et al.*, 2008; Kraut & Feudel, 2002], are observed and found, that belong respectively to different subjects, such as fluid mechanics [Aubry *et al.*, 1988], neurology [Dtchetgnia Djeundam *et al.*, 2013], biology [Billings & Schwartz, 2002], stochastic stability of structures [Roy, 1996], population ecology [Ellner & Turchin, 1995], chemistry [Naeh *et al.*, 1990], laser theory [Zhou *et al.*, 2003], communications theory [Hunt *et al.*, 1996] and so on. It is noted that for a nonlinear dynamical system which has structural

†Author for correspondence

Int. J. Bifurcation Chaos 2017.27. Downloaded from www.worldscientific.com
by HONG KONG POLYTECHNIC UNIVERSITY on 04/20/19. Re-use and distribution is strictly not permitted, except for Open Access articles.

instability, even a small noise may result in these kinds of phenomena. Thus far, most research methods emphasized on the numerical evaluation of the maximal Lyapunov exponent [He & Habib, 2013; Lin & Young, 2008; Aubry *et al.*, 1988; Dtchetgnia Djeundam *et al.*, 2013; Ellner & Turchin, 1995], which is used to characterize the chaotic properties of signals, and the fractal dimensions [Tél *et al.*, 2008; Hunt *et al.*, 1996], Stone and Holmes investigated the behaviors of the heteroclinic networks under random perturbations [Aubry *et al.*, 1988], a noise-induced transition from a periodic motion to a quasi-periodic or chaotic motion was found numerically in a Rayleigh–Duffing system [Hikihara *et al.*, 2012] and furthermore via a reduced-order Fokker–Planck–Kolmogorov (FPK) equation, a disappearance of a noise-induced energy localization was found within a monostable Duffing system. In [Roy, 1997a; Roy & Nauman, 1995], noise-induced chaos or intermittent switching behavior was found in multistable piecewise linear systems, however under the assumption of elliptic orbits and a two-dimensional Itô system, this phenomenon cannot be analyzed analytically. According to the recent researches by the authors, for a noise-excited piecewise linear system, a chaotic saddle was found to exist among a wide range of parameters [Kong *et al.*, 2016], which reflects the fact that within the same range of parameters, noise-induced chaos can exist.

Recently, the concept of quasi-potential was always used to characterize these complicated phenomena, especially for the nonlinear system which exhibits transient chaos or unattractive chaotic attractors. The unattractive chaotic attractors were found to be very common in a periodic window, and the quasi-potential plateaus caused by chaotic saddles were also observed [Kraut & Feudel, 2003b] (see Figs. 4–6 in [Kraut & Feudel, 2003b]). The quasi-potential was first introduced by Freidlin and Wentzell [2012], in order to investigate the behavior of dynamical systems that were under random perturbation. However, up till now, the method of quasi-potential is mostly used in the numerical simulations of the complicated nonlinear dynamical systems which exhibit chaos or chaotic saddles, and the reason is simply because the dynamical structures of the nonlinear stochastic systems that process these phenomena are complicated. Furthermore, the quasi-potential was used by some researchers to measure MFPT. In the study of stability problem, stochastic stability is always defined as the stability of invariant density [Young, 1986], and an oscillator can be called stochastically unstable if the MFPT is finite [Klosek-Dygas *et al.*, 1988]. In this paper, the phenomenon of noise-induced chaos obviously implies the stochastic instability of a regular attractor, and MFPT can characterize the enhancement of noise-induced escape if the chaotic saddles exist [Hong *et al.*, 2010].

Based on the previous work of the authors [Kong *et al.*, 2016], a piecewise linear system is investigated again in the present paper, for which the phenomenon of noise-induced chaos is investigated furthermore. To measure the complicated phenomenon quantitatively, a high-dimensional Itô system is obtained and the relevant MFPT is estimated via the singular perturbation method. In the present analysis, the effect of boundary layer is considered, which reflects the algebraic rate of change of MFPT with respect to time, and as a result, the more precise estimation of MFPT is then obtained. Whereas, within the analysis process the authors are challenged, wherein an ill-conditioned matrix arises and hinders the estimation of the MFPT. To solve the problem, by ignoring that term in the formula of MFPT, which relates to the ill-conditioned matrix, an approximate result is obtained. Despite its complex forms, the approximate analytical result reflects successfully the influence of chaotic saddles on the exit behavior and matches the numerical results well.

This paper is organized as follows. In Sec. 2, in the absence of noise excitation, the global dynamical properties of the piecewise linear system driven by only a harmonic excitation are illustrated by using GCMD. In Sec. 3, for the system driven by both a harmonic excitation and a Gaussian white noise, an averaged four-dimensional Itô system is obtained via the stochastic averaging method. Based on the analysis upon the boundary layer function and the rays method, the solution of the FPK equation is obtained along each ray by solving a set of ordinary differential equations (ODEs) which are formulated in Sec. 4. In Sec. 5, on the basis of Laplace approximation method and the work of Z. Schuss and his co-workers, the expression for the MFPT is formulated. As noted before, the ill-conditioned matrix induced by the term within the expression of MFPT arises, to solve the problem, one more approximation method is applied,

Int. J. Bifurcation Chaos 2017.27. Downloaded from www.worldscientific.com
by HONG KONG POLYTECHNIC UNIVERSITY on 04/20/19. Re-use and distribution is strictly not permitted, except for Open Access articles.

and finally, a comparison between the approximate result and the numerical result simulated by Monte Carlo method is given. The conclusions and some discussions are summarized in Sec. 6.

2. Global Analysis

In this section, the global dynamical properties for a deterministic piecewise linear system is investigated in advance by using GCMD, prior to the investigation on the MFPT of the relevant stochastic system, because of the complexity of the dynamical behaviors. GCMD is known as a powerful numerical method for inspecting and illustrating the global and local properties of a dynamical system [Kong *et al.*, 2016; Hong, 2010; Hong *et al.*, 2010; Han *et al.*, 2015; Han *et al.*, 2014; Yue *et al.*, 2012; Hong & Xu, 2003; Hsu, 1995; Dellnitz *et al.*, 2001]. And some efficient algorithms were devised for obtaining invariant sets in high-dimensional systems [Dellnitz *et al.*, 2001]. For the piecewise linear system, its equation of motion is given by

$$\frac{\mathrm{d}^2x}{\mathrm{d}t^2} + 2\zeta\frac{\mathrm{d}x}{\mathrm{d}t} + f(x) = F(t) \tag{1}$$

where $f(x)$ is a piecewise linear restoring force, which is defined as

$$f(x) = \begin{cases} x+1, & x \le -1, \\ 0, & |x| < 1, \\ x-1, & x \ge 1 \end{cases} \tag{2}$$

and $F(t)$ is the external excitation, i.e.

$$F(t) = f_0 + f_1\cos(\omega t) + \xi(t) \tag{3}$$

$\xi(t)$ is the random process that has a zero mean and the autocorrelation function $\langle\xi(t)\xi(t+\tau)\rangle = 2D\delta(t)$, and D is assumed as a small parameter. In mechanical systems, there are many buffers, barriers and elastic stops to limit the amplitude of vibrations, such as vibration dampers in a vehicle and fenders. And the clearance or backlash between gears cannot be avoided to model the vibration of gear lapping system. All these systems are subjected to piecewise linear restoring forces. Equation (1) is a classical and generalized model with a clearance type nonlinearity used to model many systems in practical engineering projects, especially the vibration and impact systems within mechanical and civil engineering. In this piecewise linear system, many complicated dynamical behaviors have been found.

In [Kong *et al.*, 2016], the dynamics of a deterministic piecewise linear system are investigated numerically. Through the Monte Carlo simulation, the noise-induced chaos is found twice if the frequency of the external excitation ω is around 0.49 or belongs to the interval [0.7, 1.4], thus $\omega = 0.89$ is chosen to be as the typical case to show this phenomenon numerically. In the remainder of this research, the values of some parameters are set as $\zeta = 0.01$, $f_0 = f_1 = 0.25$. For the system defined in Eq. (1) excited by a very small noise, Fig. 1 displays the signal history and the corresponding projection

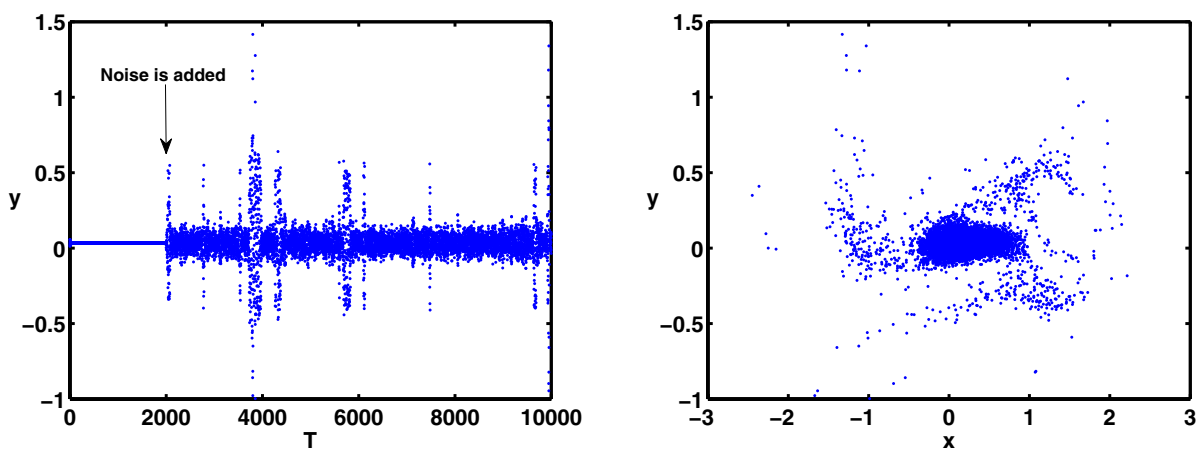

(a) (b)

Fig. 1. (a) The time history of y-component of the Poincaré points on (4) are shown versus the time T which stands for the period of the external excitation $T = 2\pi/\omega$ and (b) the projection of the same signal onto the Poincaré section (4). $\omega = 0.89$, $D = 6e-5$ are chosen in this figure.

Int. J. Bifurcation Chaos 2017.27. Downloaded from www.worldscientific.com
by HONG KONG POLYTECHNIC UNIVERSITY on 04/20/19. Re-use and distribution is strictly not permitted, except for Open Access articles.

on a Poincaré section, which is defined by

$$\Sigma = \left\{ (x, y, t) \,|\, t = t_0, \ \mathrm{mod}\ \frac{2\pi}{\omega} \right\} \tag{4}$$

where y-coordinate denotes $\dot{x}$. The comparison between the signal in Fig. 1(a) before and after noise is added, the fact that the chaotic saddle exists in the deterministic system and the fact that the phenomenon of noise-induced chaos exists in the stochastic system are both verified. And the projection of this signal is displayed in Fig. 1(b).

Due to the complexity of the dynamical behaviors of the system defined in Eq. (1), in this section the GCMD method is applied to find the refined structure of the phase portrait on the Poincaré section defined in Eq. (4), in the case of no noise excitation (i.e. $D = 0$). The GCMD method is a numerical method which is based on the generalized cell-mapping (GCM) method [Hsu, 1995, 1987] and graph theory, and with the help of the theory of digraph, this method extracts much more information through numerical computation, such as attractors, saddles and even chaotic saddles. Although via this method, the accurate positions of the fixed points cannot be obtained, the areas that they occupy are given, which are sufficient for the qualitative analysis.

In Fig. 2, the green parts are two period-1 attractors, the black parts are the regular and chaotic saddles, and the blue and red parts are the stable and unstable manifolds of saddles respectively. The remaining pictures in this paper

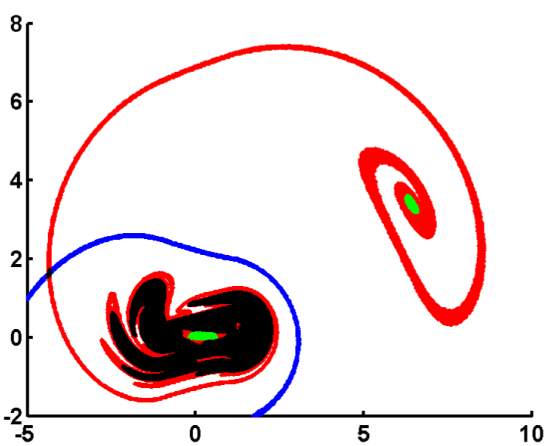

Fig. 2. The phase diagram projected on the Poincaré section by using GCMD method, $\omega = 0.89$. The attractors are shown by green points, and the saddle and chaotic saddles are shown by black points. The blue and red points are the stable and unstable manifolds of saddles respectively.

obtained from the GCMD method follow the same convention. A cell space of 2000×2000 is used to cover the phase diagram in Fig. 2, and there are one period-1 stable solution with a large amplitude (the green part in the upper right), one period-1 stable solution with a small amplitude (the green part in the lower left), one period-1 saddle (the black point located in the insertion of the blue and red line in the left) and one big black part that has a refined structure which is a chaotic saddle. This chaotic saddle is a set of saddles interconnected by the manifold of each other [Kong *et al.*, 2016; Hong & Xu, 2003]. It is noted that if the resolution of this method is raised extremely, each of the two period-1 stable solutions and the period-1 saddle solution depicted in Fig. 2 should turn out to be a point respectively on the phase portrait, however the simulation process is uneconomical. Because the purpose of the investigation here is to just show the global properties of this system, not to determine the exact positions of these solutions, the results shown in Fig. 2 are enough here.

By comparing Fig. 1(b) and the chaotic saddle in Fig. 2, it is observed that the phenomenon of noise-induced chaos is a kind of exit problem in which the system status exits from the basin of the stable attractor to the chaotic saddle under even a small noise excitation. That is how the noise-induced chaos occurs. Furthermore, due to the nonattracting property of the chaotic saddle, it is impossible for the system to stay at the chaotic saddle for a long time, instead it moves back to the stable attractor intermittently. The intermittent switching behavior occurs, as a result. So, the noise-induced chaos is a kind of exit behavior for dynamical systems wherein the attractors and the chaotic saddles coexist. And we note that in general, noise-induced chaos is not only a simple transition between chaotic saddles and regular attractors. For example, Lin and Young studied noise-induced chaos without intermittent switching behavior in a two-dimensional system [Lin & Young, 2008].

In order to characterize both the attractor and the chaotic saddle, a further analysis is required with a smaller scope and a finer resolution. Figure 3(a) shows the refined structure just around the period-1 stable solution with a small amplitude. In this small scale, it is easy to find that there is a period-3 saddle [three black parts connected to each other in Fig. 3(a)] around the attractor, which demonstrates that the period-3 saddle is the nearest

Int. J. Bifurcation Chaos 2017.27. Downloaded from www.worldscientific.com
by HONG KONG POLYTECHNIC UNIVERSITY on 04/20/19. Re-use and distribution is strictly not permitted, except for Open Access articles.

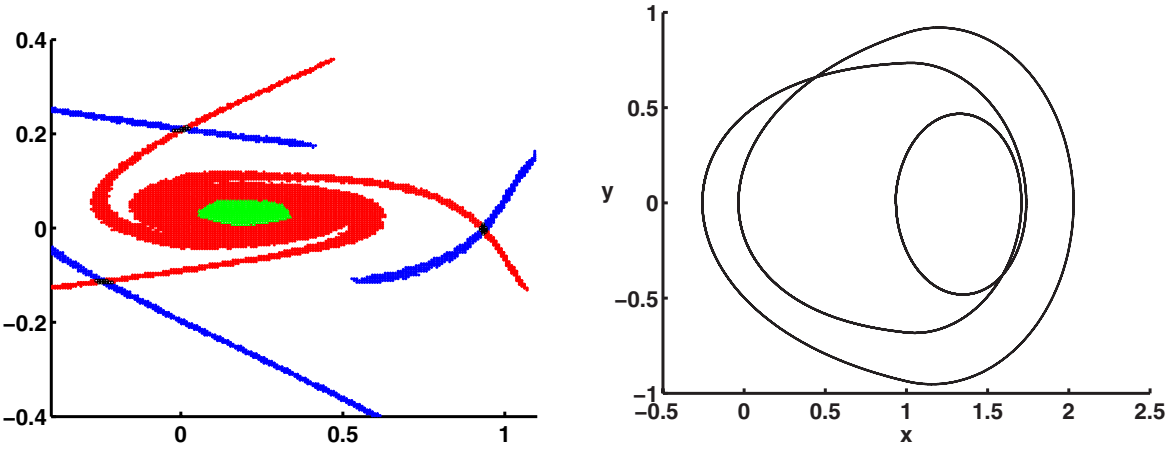

(a) (b)

Fig. 3. (a) The phase diagram projected on the Poincaré section (4) in a small scale around the period-1 stable cycle with a small amplitude by using GCMD method at $\omega = 0.89$ and (b) the two-dimensional phase trajectory on (x, y) plane which is integrated numerically by choosing the right black point in Fig. 3(a) as the initial point.

part of the chaotic saddle from period-1 attractor and corresponds to the edge of the quasi-potential plateau [Kraut & Feudel, 2003b; Hunt *et al.*, 1996]. Choosing the right black point on the Poincaré section as the initial point, the trajectory of this period-3 saddle is obtained numerically and plotted in Fig. 3(b). Thus, we expect the analysis of the phenomenon of noise-induced chaos can be replaced by the analysis of the transition between the period-1 attractor and the period-3 saddle.

3. Simplification of the System

Through the global analysis by GCMD method in Sec. 2, one period-3 saddle is found just around the period-1 attractor which corresponds to the edge of quasi-potential plateau. Thus, the analysis on the phenomenon of noise-induced chaos can be replaced by the analysis on the exit behavior between this period-3 saddle and the period-1 attractor. Since both the white noise excitation and the damping coefficient of the system are small, the stochastic averaging method, which is used widely for the analysis of the exit problems [Roy, 1996, 1997b, 1994b, 1997a, 1994a, 1995; Rodrigues *et al.*, 2010; Chen & Zhu, 2010; Chen *et al.*, 2009], can be applied to simplify the system (1). It is noted that the period-1 attractor and this period-3 saddle are both structurally stable, thus it is reasonable to use an approximation method, such as the stochastic averaging method, to deal with this exit problem [Guckenheimer & Holmes, 1983], and the averaged system as the substitution of the original piecewise linear system will facilitate the analysis of the MFPT.

Via the comparison between the trajectory depicted in Fig. 3(b) and an elliptic trajectory, it is clear that the amplitude of this trajectory is obviously period-3. Then, the power spectrum of the motion around the period-3 saddle displayed in Fig. 4 shows that the subharmonic frequencies of orders 1/3 and 2/3 are present beside the main oscillating frequency. Thus, by adding two period-3 harmonic components to the amplitude of the elliptic trajectory, the approximate solution to Eq. (1)

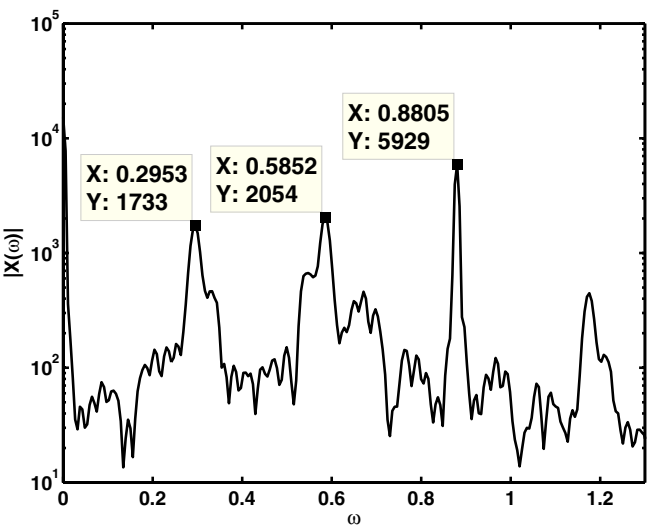

Fig. 4. The power spectrum of the motion around the period-3 saddle found in Fig. 3.

Int. J. Bifurcation Chaos 2017.27. Downloaded from www.worldscientific.com
by HONG KONG POLYTECHNIC UNIVERSITY on 04/20/19. Re-use and distribution is strictly not permitted, except for Open Access articles.

is assumed as follows

$$x(t) = c + r(t)\cos(\omega t + \theta(t)) + r_3(t)\cos\left(\frac{2\omega t}{3} + \vartheta(t)\right) + r_{13}(t)\cos\left(\frac{\omega}{3} + \Theta(t)\right) \quad (5)$$

where c is a constant which is used to express the offset of the trajectory caused by the constant force f_0, r is the amplitude of the period-1 component, r_3 and r_{13} are the amplitudes of the period-3 components respectively, and θ, ϑ and Θ are the phases of these components, respectively. However the seven independent variables contained in Eq. (5) will lead to much difficulty in the following calculation. Since the last term in Eq. (5) is the one with the minimum energy according to Fig. 4, it is reasonable to ignore the last term to simplify the following calculation. And the following results shown in Fig. 6 demonstrate that this approximation is appropriate and valid. Then, the new approximate solution is given below

$$\begin{cases} x(t) = c + r(t)\cos(\omega t + \theta(t)) + r_3(t)\cos\left(\dfrac{2\omega t}{3} + \vartheta(t)\right) \\ \qquad = c + a(t)\cos(\omega t) - b(t)\sin(\omega t) + d(t)\cos\left(\dfrac{2\omega t}{3}\right) - e(t)\sin\left(\dfrac{2\omega t}{3}\right), \\ y(t) = -\omega r(t)\sin(\omega t + \theta(t)) - \dfrac{2\omega}{3} r_3(t)\sin\left(\dfrac{2\omega t}{3} + \vartheta(t)\right) \\ \qquad = -\omega[a(t)\sin(\omega t) + b(t)\cos(\omega t)] - \dfrac{2\omega}{3}\left[d(t)\sin\left(\dfrac{2\omega t}{3}\right) + e(t)\cos\left(\dfrac{2\omega t}{3}\right)\right]. \end{cases} \quad (6)$$

The van der Pol variables a, b, c, d, and e are introduced to transform the periodic solutions in the phase space (x, y) to the fixed points in the van der Pol phase space (a, b, c, d, e). Via the comparison between Figs. 6(b) and 3(b), it is easy to verify that the expressions in Eq. (6) give well the approximations of either the period-3 solution [comparing Fig. 6(b) with Fig. 3(b)] under the condition that $r_3(t) \neq 0$ or $d(t)e(t) \neq 0$ or the period-1 solution if $r_3(t) = 0$ or $d(t) = 0, e(t) = 0$ [He & Habib, 2013; Roy & Nauman, 1995]. With the assumption of the approximate solution given in Eq. (6), it is reasonable to consider all the variables of a, b, c, d, and e as slow variables.

Next, the piecewise linear function defined in Eq. (2) is expanded along the trajectories given by Eq. (6) [Roy, 1997b], for which the expansion is given by

$$f(x(t)) = N_0 + N_1\cos\left(\frac{2\omega t}{3}\right) + N_2\sin\left(\frac{2\omega t}{3}\right) + N_3\cos(\omega t) + N_4\sin(\omega t) \quad (7)$$

where each of N_i, $i = 0, \ldots, 4$ is the piecewise function of the van der Pol variables c, a, b, d, and e and can be obtained easily through a simple integral of $f(x)$ or $f(x)$ multiples of an orthogonal triangle, if c, a, b, d, and e are given, i.e.

$$\begin{cases} N_0 = \dfrac{\omega}{6\pi}\displaystyle\int_0^{6\pi/\omega} f(x)\mathrm{d}t, \\ N_{2i-1} = \dfrac{\omega}{3\pi}\displaystyle\int_0^{6\pi/\omega} f(x)\cos\left(\dfrac{(i+1)\,\omega t}{3}\right)\mathrm{d}t, \quad \text{for } i = 1, 2. \\ N_{2i} = \dfrac{\omega}{3\pi}\displaystyle\int_0^{6\pi/\omega} f(x)\sin\left(\dfrac{(i+1)\omega t}{3}\right)\mathrm{d}t. \end{cases} \quad (8)$$

Since N_0, N_1, N_2, N_3, N_4 are all piecewise and nonsmooth functions, wherein the variations of N_0 and N_2 versus the variables a are displayed in Fig. 5, then the approximation expression given in Eq. (7) is still

Int. J. Bifurcation Chaos 2017.27. Downloaded from www.worldscientific.com
by HONG KONG POLYTECHNIC UNIVERSITY on 04/20/19. Re-use and distribution is strictly not permitted, except for Open Access articles.

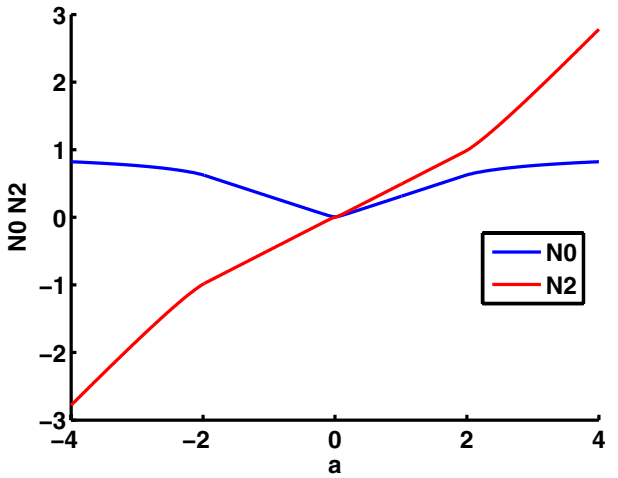

Fig. 5. The multivariate functions $N_0(c, a, b, d, e)$, $N_2(c, a, b, d, e)$ plotted versus the variable a.

piecewise and nonsmooth in the van der Pol variable space, just like that given in Eq. (2), which is the piecewise and nonsmooth function of the state variable.

Consider the state equations for Eq. (1), as given by

$$\begin{cases} \dot{x}(t) = y(t), \\ \dot{y}(t) + 2\zeta y(t) + f(x) = F(t). \end{cases} \tag{9}$$

After substituting Eq. (6) into Eq. (9) through a series of algebraic calculations, four governing equations on the variables of (a, b, d, e) are obtained. Then the substitutions of Eqs. (7) and (3) into Eq. (9) and the application of the stochastic averaging method lead to a set of averaged Itô stochastic differential equations, i.e.

$$\begin{cases} \mathrm{d}a(t) = \dfrac{1}{2}\dfrac{\omega^2 b(t) + N_4 - 2\zeta a(t)\omega}{\omega}\mathrm{d}t + \dfrac{\sqrt{D}}{\omega}\mathrm{d}W_1(t), \\ \mathrm{d}b(t) = \dfrac{1}{2}\dfrac{-2\zeta b(t)\omega + N_3 - f_1 - \omega^2 a(t)}{\omega}\mathrm{d}t + \dfrac{\sqrt{D}}{\omega}\mathrm{d}W_2(t), \\ \mathrm{d}d(t) = \dfrac{1}{12}\dfrac{9N_2 + 4\omega^2 e(t) - 12d(t)\omega\zeta}{\omega}\mathrm{d}t + \dfrac{3\sqrt{D}}{2\omega}\mathrm{d}W_3(t), \\ \mathrm{d}e(t) = \dfrac{1}{12}\dfrac{-12\zeta e(t)\omega - 4\omega^2 d(t) + 9N_1}{\omega}\mathrm{d}t + \dfrac{3\sqrt{D}}{2\omega}\mathrm{d}W_4(t), \end{cases} \tag{10}$$

where each $W_i(t)$ for $i = 1, \ldots, 4$ is an unit Wiener process.

However Eq. (10) is not complete, there is a lack of governing equation for the van der Pol variable c, which is an algebraic one and is obtained through the condition that the integral average value of $\ddot{c}(t)$ over

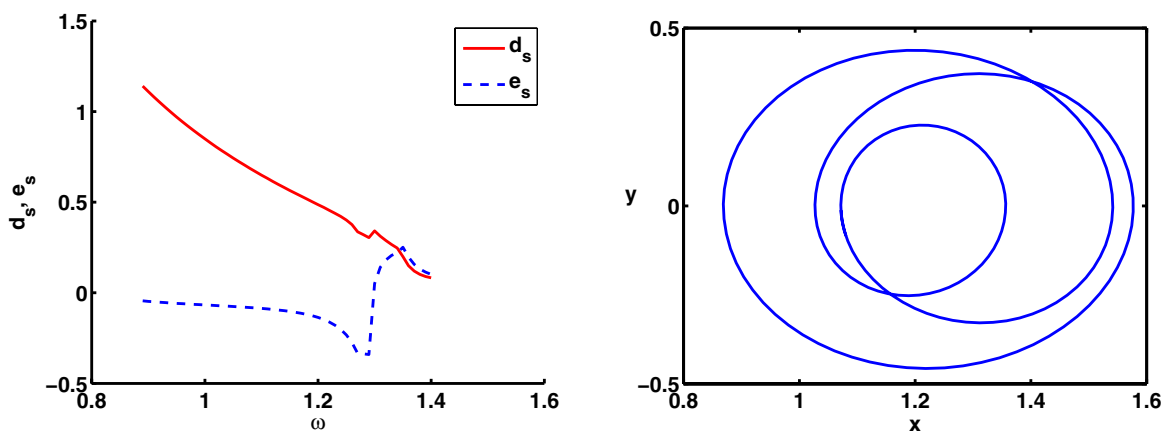

(a) (b)

Fig. 6. (a) Nonvanishing d_s, e_s of the solutions of Eq. (13) are plotted versus ω and (b) the two-dimensional phase trajectory on (x, y) plane corresponding to the period-3 saddle when $\omega = 1.4$.

Int. J. Bifurcation Chaos 2017.27. Downloaded from www.worldscientific.com
by HONG KONG POLYTECHNIC UNIVERSITY on 04/20/19. Re-use and distribution is strictly not permitted, except for Open Access articles.

the interval of $[0, 6\pi/\omega]$ for the variable t vanishes, i.e.

$$\frac{\omega}{6\pi}\int_0^{6\pi/\omega}\left\{\ddot{x}(t)+\omega^2\left[a\cos(\omega t)-b\sin(\omega t)+\frac{4}{9}\left(d\cos\left(\frac{2}{3}\omega t\right)-e\sin\left(\frac{2}{3}\omega t\right)\right)\right]\right\}\mathrm{d}t=0. \tag{11}$$

By substituting Eqs. (1), (3) and (7) into Eq. (11), the algebraic equation is then obtained, i.e.

$$N_0 = f_0. \tag{12}$$

With Eqs. (10) and (12), a complete set of governing equations for (a, b, c, d, e) is gained, which, under the assumption given in Eq. (6), is an Itô system with a higher dimension than those of the Itô system considered in [Roy, 1997a; Roy & Nauman, 1995]. Based upon this system, the phenomenon of noise-induced chaos is predicted.

Firstly, the nonlinear deterministic version of the averaged equations is considered, to which c_s, a_s, b_s, d_s, and e_s represent the steady-state solutions. The equations are given by

$$\begin{cases}\dfrac{\omega^2 b_s + N_4 - 2\zeta a_s\omega}{2\omega} = 0,\\[2ex] \dfrac{-2\zeta b_s\omega + N_3 - f_1 - \omega^2 a_s}{2\omega} = 0,\\[2ex] \dfrac{9N_2 + 4\omega^2 e_s - 12 d_s\omega\zeta}{12\omega} = 0,\\[2ex] \dfrac{-12\zeta e_s\omega - 4\omega^2 d_s + 9N_1}{12\omega} = 0,\\[2ex] N_0(a_s, b_s, c_s, d_s, e_s) - f_0 = 0.\end{cases} \tag{13}$$

It is noted that the hyperbolic fixed points of the averaged system correspond to the hyperbolic periodic orbits in the original system, respectively [Guckenheimer & Holmes, 1983]. Among all the three solutions to Eq. (13), there is only one solution possessing the nonvanishing d_s and e_s, which are the functions of ω and are depicted in Fig. 6(a), and under the condition that $\omega = 1.4$, the two-dimensional phase trajectory on (x, y) plane, which corresponds to the period-3 saddle, is shown in Fig. 6(b).

4. Estimation of the Stationary Probability Density Function

In Sec. 4, the stationary probability density function of the four-dimensional Itô system that is defined in Eq. (10) is investigated in D, which is the domain of interest and is completely inside the basin of attraction of the stable equilibrium point mentioned above [Fig. 3(a) shows that the basin of attraction is very small]. The boundary of D is denoted by ∂D.

Suppose that $\mathbf{x}_0$ is a five-dimensional vector, which is defined by

$$\mathbf{x}_0 = [x_1 \quad x_2 \quad x_3 \quad x_4 \quad x_5]^T = [a \quad b \quad d \quad e \quad c]^T. \tag{14}$$

Since x_5 is governed by the algebraic equation (12), then x_5 is a function of x_1, x_2, x_3, x_4. Thus the vector stochastic process of $\mathbf{x} = [x_1 \quad x_2 \quad x_3 \quad x_4]^T$, which is defined by Eq. (10), forms a vector diffusion process and its stationary probability density function $p(\mathbf{x})$ satisfies the following FPK equation

$$\begin{cases} L[p(\mathbf{x})] \\ \quad = \displaystyle\sum_{i,j=1}^{4}\left\{-\partial_i[b_i(\mathbf{x})p(\mathbf{x})] + \frac{\epsilon}{2}\partial_{ij}^2[a_{ij}(\mathbf{x})p(\mathbf{x})]\right\} = 0,\\ \partial_i = \dfrac{\partial}{\partial x_i}, \quad \partial_{ij}^2 = \dfrac{\partial^2}{\partial x_i \partial x_j},\end{cases} \tag{15}$$

where $\epsilon = D/\omega^2$ is a small quantity, and b_i and a_{ij} are respectively the drift coefficients and the diffusion coefficients which are defined by

$$\begin{cases} \mathbf{A}(\mathbf{x}) = \begin{bmatrix} a_{11} & a_{12} & a_{13} & a_{14}\\ a_{21} & a_{22} & a_{23} & a_{24}\\ a_{31} & a_{32} & a_{33} & a_{34}\\ a_{41} & a_{42} & a_{43} & a_{44}\end{bmatrix} = \begin{bmatrix} 1 & 0 & 0 & 0\\ 0 & 1 & 0 & 0\\ 0 & 0 & \frac{9}{4} & 0\\ 0 & 0 & 0 & \frac{9}{4}\end{bmatrix},\\ b_1(\mathbf{x}) = \dfrac{1}{2}\dfrac{\omega^2 b + N_4(\mathbf{x}) - 2\zeta a\omega}{\omega},\\ b_2(\mathbf{x}) = \dfrac{1}{2}\dfrac{-2\zeta b\omega + N_3(\mathbf{x}) - f_1 - \omega^2 a}{\omega},\\ b_3(\mathbf{x}) = \dfrac{1}{12}\dfrac{9N_2(\mathbf{x}) + 4\omega^2 e - 12 d\omega\zeta}{\omega},\\ b_4(\mathbf{x}) = \dfrac{1}{12}\dfrac{-12\zeta e\omega - 4\omega^2 d + 9N_1(\mathbf{x})}{\omega}.\end{cases} \tag{16}$$

Int. J. Bifurcation Chaos 2017.27. Downloaded from www.worldscientific.com
by HONG KONG POLYTECHNIC UNIVERSITY on 04/20/19. Re-use and distribution is strictly not permitted, except for Open Access articles.

For the matrix $\mathbf{A}$, $a_{ij} = 0$ for $i \neq j$, $i, j = 1, \ldots, 4$, and $a_{ii} \neq 0$ for $i = 1, \ldots, 4$. This particular simplification is suitable for all the systems that are under the external random excitations, and dramatically reduces the complexity of the solution process for the FPK equation (15).

For $p(\mathbf{x})$, the normalization condition and boundary condition are respectively given by

$$\int_{\mathrm{R}^5} p(\mathbf{x})\mathrm{d}\mathbf{x} = 1, \tag{17}$$

$$p(\mathbf{x}) = 0, \quad \mathbf{x} \in \partial\mathrm{D}. \tag{18}$$

In order to find the solution to the FPK equation (15) in the limit $\epsilon \to 0$, the Wenzel–Kramers–Brillouin (WKB) approximation is applied and based on which, the approximation of the expression of the stationary probability density function asymptotically is assumed as

$$p(\mathbf{x}) = w(\mathbf{x}) \exp\left[-\frac{\psi(\mathbf{x})}{\epsilon} + O(\epsilon)\right] q(\mathbf{x}) \tag{19}$$

wherein the function $\psi(\mathbf{x})$ is the quasi-potential function, $w(\mathbf{x})$ is a prefactor function and $q(\mathbf{x})$ is the boundary layer function which satisfies the following condition

$$\begin{cases} q(\mathbf{x}) = 0, & \mathbf{x} \in \tilde{\mathrm{D}}, \\ q(\mathbf{x}) = 1, & \mathbf{x} \notin \tilde{\mathrm{D}}, \end{cases} \tag{20}$$

where $\tilde{\mathrm{D}}$ denotes a thin boundary layer close to the boundary $\partial\mathrm{D}$. It is impossible to obtain the solution over the entire R^4, however the solution over the domain D is investigated instead.

By substituting Eq. (19) into Eq. (15), the following equation is obtained

$$\begin{cases} q(\mathbf{x})L(z(\mathbf{x},\epsilon)) - z(\mathbf{x},\epsilon)\overline{L}(\psi(\mathbf{x})) \\ \qquad + \epsilon \sum_{i=1}^{4} a_{ii}\partial_i\psi(\mathbf{x})\partial_i z(\mathbf{x},\epsilon) = 0, \\ z(\mathbf{x},\epsilon) = w(\mathbf{x}) \exp\left(-\dfrac{\psi(\mathbf{x})}{\epsilon}\right), \end{cases} \tag{21}$$

where under the condition that $a_{ij} = 0$ for $i \neq j$, $i, j = 1, \ldots, 4$, the operator $\overline{L}$ is the substitution of the adjoint operator of the Fokker–Planck operator L defined in Eq. (15), i.e.

$$\overline{L} = \sum_{i=1}^{4} b_i\partial_i + \frac{1}{2}\epsilon \sum_{i}^{4} a_{ii}\partial_{ii}^2. \tag{22}$$

Based on Eq. (20), Eq. (21) is divided into two equations, i.e.

$$\begin{cases} L[z(\mathbf{x},\epsilon)] = 0, \quad \mathbf{x} \notin \tilde{\mathrm{D}}, \\ -z(\mathbf{x},\epsilon)\overline{L}(q(\mathbf{x})) + \epsilon \sum_{i=1}^{4} a_{ii}\partial_i q(\mathbf{x})\partial_i z(\mathbf{x},\epsilon) = 0, \\ \qquad\qquad\qquad\qquad\qquad\qquad \mathbf{x} \in \tilde{\mathrm{D}}, \end{cases} \tag{23}$$

which means that the first term of Eq. (21) vanishes outside the boundary layer and the other terms vanish inside the boundary layer.

The solution to the first equation of Eq. (23) is then investigated. By expanding the first equation of Eq. (23) and identifying the terms of the order ϵ^{-1} and ϵ^0, two independent partial differential equations of the first order are obtained, the one that governs $\psi(\mathbf{x})$ is the Hamilton–Jacobi equation

$$\overline{L}(\psi(\mathbf{x})) = 0 \tag{24}$$

and the other one that governs $w(\mathbf{x})$ is the transport equation

$$-\sum_{i=1}^{4} ((b_i(\mathbf{x}) + a_{ii}\partial_i\psi(\mathbf{x}))\partial_i w(\mathbf{x})) - \sum_{i=1}^{4} \left(\partial_i b_i(\mathbf{x}) + \frac{1}{2}a_{ii}\partial_{ii}^2\psi(\mathbf{x})\right) w(\mathbf{x}) = 0. \tag{25}$$

Based on the theory of partial differential equation of the first order, Eqs. (24) and (25) are both solvable by using the rays method [Ludwig, 1975]. The rays of these two equations are governed by ordinary differential equations, and along each ray $\psi(\mathbf{x})$ and $w(\mathbf{x})$ are also governed by ordinary differential equations respectively. With appropriate initial conditions, a family of rays is found to cover the domain D, and then, approximate stationary probability density function is obtained in the domain D. The equations governing the rays of Eq. (24) are given below

$$\begin{cases} \dot{x}_i = b_i(\mathbf{x}) + a_{ii}p_i(\mathbf{x}), \\ \dot{p}_i = -\sum_{j=1}^{4} (\partial_i b_j(\mathbf{x})p_j(\mathbf{x})), \end{cases} \quad \text{for } i = 1, \ldots, 4, \tag{26}$$

where $p_i(\mathbf{x}) = \partial_i\psi(\mathbf{x})$. Supposing that the coordinate along the rays is denoted by s, then $\dot{x}_i, \dot{p}_i$ are

Int. J. Bifurcation Chaos 2017.27. Downloaded from www.worldscientific.com
by HONG KONG POLYTECHNIC UNIVERSITY on 04/20/19. Re-use and distribution is strictly not permitted, except for Open Access articles.

respectively defined by $\dot{x}_i = \frac{\mathrm{d}x_i}{\mathrm{d}s}$, $\dot{p}_i = \frac{\partial^2\psi(\mathbf{x})}{\partial x_i \partial s}$. Along each ray, $\psi(\mathbf{x})$ is governed by

$$\dot{\psi} = \frac{1}{2}\sum_{i=1}^{4} a_{ii} p_i^2. \tag{27}$$

With Eqs. (26) and (27), a family of rays that covers the whole domain of D is first obtained, and then the function of $\psi(\mathbf{x})$ on each ray is determined.

Via the same method, the rays defined by Eq. (25) are obtained which are the same as those that are given by Eq. (26). Along each of the rays, $w(\mathbf{x})$ is governed by

$$\dot{w} = -\sum_{i=1}^{4}\left[\partial_i b_i(\mathbf{x}) + \frac{1}{2}a_{ii}\partial_i p_i(\mathbf{x})\right] w(\mathbf{x}). \tag{28}$$

It is noted that Eq. (28) is different from Eq. (27), for Eq. (28) there are second partial derivatives of $\psi(\mathbf{x})$ involved, thus $w(\mathbf{x})$ cannot be determined by Eqs. (26) and (28).

To determine these second partial derivatives of $\psi(\mathbf{x})$, each equation in Eq. (26) needs to be differentiated with respect to the three coordinates of the four-dimensional space where the rays lie, i.e. θ, φ, ϕ. Thus, along each ray, 24 ODEs are obtained, i.e.

$$\begin{cases}
\dot{l}_i = \partial_\theta \dot{x}_i = \sum_{j=1}^{4} l_j \partial_j b_i + a_{ii} q_i, \\
\dot{m}_i = \partial_\varphi \dot{x}_i = \sum_{j=1}^{4} m_j \partial_j b_i + a_{ii} r_i, \\
\dot{n}_i = \partial_\phi \dot{x}_i = \sum_{j=1}^{4} n_j \partial_j b_i + a_{ii} s_i, \\
\dot{q}_i = \partial_\theta \dot{p}_i = -\sum_{k=1}^{4}\sum_{j=1}^{4}[(l_j \partial_{ij}^2 b_k)p_k + q_j \partial_i b_j], \\
\dot{r}_i = \partial_\varphi \dot{p}_i = -\sum_{k=1}^{4}\sum_{j=1}^{4}[(m_j \partial_{ij}^2 b_k)p_k + r_j \partial_i b_j], \\
\dot{s}_i = \partial_\varphi \dot{p}_i = -\sum_{k=1}^{4}\sum_{j=1}^{4}[(m_j \partial_{ij}^2 b_k)p_k + r_j \partial_i b_j],
\end{cases} \quad \text{for } i = 1, \ldots, 4. \tag{29}$$

However, the second partial derivatives that arise in Eq. (28) cannot be solved directly from the above 24 ODEs, but from the following relationships based on the chain rule, i.e.

$$q_i = \sum_{j=1}^{4} l_j \partial_{ij}^2 \psi, \quad r_i = \sum_{j=1}^{4} m_j \partial_{ij}^2 \psi, \quad s_i = \sum_{j=1}^{4} n_j \partial_{ij}^2 \psi, \quad \dot{p}_i = \sum_{j=1}^{4} \dot{x}_j \partial_{ij}^2 \psi, \quad \text{for } i = 1, \ldots, 4. \tag{30}$$

The situation now is that the 12 second partial derivatives of ψ should be solved from the 16 linear algebraic equations, which is obviously overconstrained, so the least square method is applied here. Denote the inhomogeneous term and the coefficient matrix of the above linear equations by $\mathbf{N}$ and $\mathbf{C}$ respectively, then the solution vector $\mathbf{x}$ which consists of 12 second partial derivatives of ψ is evaluated by

$$\mathbf{X} = (\mathbf{C}^{\mathrm{T}}\mathbf{C})^{-1}\mathbf{C}\mathbf{N}. \tag{31}$$

Thus far, 34 ODEs are obtained from the combination of Eqs. (26), (29) and (30), however the corresponding initial conditions are missing, which, according to characteristics theory of first order partial differential equation [Ludwig, 1975], will be discussed on a small hypersphere in R^4 with radius α.

Int. J. Bifurcation Chaos 2017.27. Downloaded from www.worldscientific.com
by HONG KONG POLYTECHNIC UNIVERSITY on 04/20/19. Re-use and distribution is strictly not permitted, except for Open Access articles.

Since in the limit $\alpha \to 0$, the stationary probability density function is approximately Gaussian around the stable equilibrium point, then the initial conditions are readily derived, i.e.

$$\begin{cases} x_{10} = x_1^* + \alpha \sin(\theta)\sin(\varphi)\sin(\phi), \quad x_{20} = x_2^* + \alpha \sin(\theta)\sin(\varphi)\cos(\phi), \\ x_{30} = x_3^* + \alpha \sin(\theta)\cos(\varphi), \quad x_{40} = x_4^* + \alpha \cos(\theta), \\ p_{i0} = \sum_{j=1}^{4} k_{ij}(x_{j0} - x_j^*), \quad \text{for } i = 1, \ldots, 4, \\ \psi_0 = \dfrac{1}{2}\sum_{i,j=1}^{4} k_{ij}(x_{i0} - x_i^*)(x_{j0} - x_j^*), \quad w_0 = 1, \end{cases} \tag{32}$$

where $\mathbf{x}^* = (x_1^*, x_2^*, x_3^*, x_4^*)$ is the particular stable equilibrium point given in Sec. 3 and each k_{ij} is the element of the inverse of the covariance matrix $\mathbf{S}$ which is derived from

$$\mathbf{B} = [\partial_j b_i(\mathbf{x}^*)], \quad \mathbf{BS} + \mathbf{SB} = -\mathbf{A}, \quad \mathbf{K} = \mathbf{S}^{-1}. \tag{33}$$

The other initial conditions are given as below

$$\begin{cases} l_1 = \alpha\cos(\theta)\sin(\varphi)\sin(\phi), \quad l_2 = \alpha\cos(\theta)\sin(\varphi)\cos(\phi), \quad l_3 = \alpha\cos(\theta)\cos(\varphi), \quad l_4 = -\alpha\sin(\theta), \\ m_1 = \alpha\sin(\theta)\cos(\varphi)\sin(\phi), \quad m_2 = \alpha\sin(\theta)\cos(\varphi)\cos(\phi), \quad m_3 = -\alpha\sin(\theta)\sin(\varphi), \quad m_4 = 0, \\ r_1 = \alpha\sin(\theta)\sin(\varphi)\cos(\phi), \quad r_2 = -\alpha\sin(\theta)\sin(\varphi)\sin(\phi), \quad r_3 = 0, \quad r_4 = 0, \\ n_i = \sum_{j=1}^{4} k_{ij} l_j, \quad q_i = \sum_{j=1}^{4} k_{ij} m_j, \quad s_i = \sum_{j=1}^{4} k_{ij} n_j, \quad \text{for } i = 1, \ldots, 4. \end{cases} \tag{34}$$

In brief, the solution to the first equation of Eq. (23) is obtained.

Next, the solution to the second equation in Eq. (23), which is the governing equation of the boundary layer function $q(\mathbf{x})$, is then investigated. Before the analysis, it is supposed that the boundary ∂D is noncharacteristic, which means that the following condition holds everywhere on the boundary ∂D, i.e.

$$\mathbf{b} \cdot \mathbf{v} < 0 \tag{35}$$

where $\mathbf{b}$ is the drift vector of the system (10) and $\mathbf{v}$ is the outer normal vector on the boundary ∂D. This condition is satisfied readily by choosing the domain D appropriately.

In order to analyze the boundary layer function in the thin boundary layer $\tilde{\mathrm{D}}$, two new local coordinates are introduced, $(\rho, \mathbf{s}) = (\rho, s_1, s_2, s_3)$, where $\rho = \rho(\mathbf{x})$ characterizes the distance between the point $\mathbf{x}$ and the boundary ∂D, and $\mathbf{s} = [s_1, s_2, s_3]$ are the local coordinates along the boundary. Since every point $\mathbf{x}$ near ∂D corresponds to only one ray defined by Eq. (26), then only one point $\mathbf{x}^b$ on the boundary is found via each ray, which corresponds to $\mathbf{x}$. Thus, if the condition Eq. (35) is satisfied, ρ is defined by

$$\rho(\mathbf{x}) = \psi(\mathbf{x}^b) - \psi(\mathbf{x}). \tag{36}$$

And a stretched variable needs to be introduced, i.e.

$$\mu = \frac{\rho}{\epsilon}. \tag{37}$$

Based on the new local coordinates, the new boundary layer function is then given by

$$Q(\mu, \mathbf{s}) = q(\mathbf{x}). \tag{38}$$

With the new boundary layer function and new local variables, via a simple computation and identifying the terms of the order ϵ^{-1}, a new boundary layer equation governing $Q(\mu, \mathbf{s})$ is obtained, i.e.

$$\overline{L}(\psi(\mathbf{x}))\partial_\mu Q(\mu, \mathbf{s}) + \left[\frac{1}{2}\sum_{i=1}^{4} a_{ii}(\partial_i \psi(\mathbf{x}))^2\right]\partial_{\mu\mu}^2 Q(\mu, \mathbf{s}) = 0 \tag{39}$$

of which the simple form can then be obtained, on the basis of the Hamilton–Jacobi equation (24),

Int. J. Bifurcation Chaos 2017.27. Downloaded from www.worldscientific.com
by HONG KONG POLYTECHNIC UNIVERSITY on 04/20/19. Re-use and distribution is strictly not permitted, except for Open Access articles.

i.e.

$$\partial^2_{\mu\mu} Q(\mu, \mathbf{s}) + \partial_\mu Q(\mu, \mathbf{s}) = 0. \tag{40}$$

Combined with the boundary condition given in Eq. (20), the solution is finally given by

$$Q(\mu, \mathbf{s}) = 1 - \exp(-\mu), \tag{41}$$

which is the first-order approximation of the boundary layer function.

With the boundary layer function defined in Eq. (41), the 34 ODEs given by Eqs. (26) to (29) combined with their initial conditions given by Eqs. (32) to (34) and the 16 linear equations defined in Eq. (30), the stationary probability density function defined in Eq. (19) are obtained along each ray in the domain D. Although this method leads to a set of 34 ODEs which is a little complicated, through it, the stationary probability density function for a high-dimensional Itô system is obtained, which is the preparation for the estimation of the MFPT.

5. Estimation of the MFPT

In Sec. 5 the exit problem of the noise-driven piecewise linear system that exhibits transient chaos is investigated. Based on the singular perturbed method, some results of MFPT and the distribution of exit points were given by Z. Schuss and his co-workers [Naeh *et al.*, 1990; Bobrovsky & Schuss, 1982], and the quasi-potential plateaus were found in the systems that exhibit transient chaos [Kraut & Feudel, 2003b]. In this work, based on the concept of the quasi-potential plateaus, the phenomenon of noise-induced chaos which is found in Sec. 2 is measured by MFPT. The simplified system with respect to the period-3 saddle and the period-1 attractor has been established in Sec. 3. Then, with the preparation that has been completed in Sec. 4, the phenomenon of noise-induced chaos can be studied through analyzing the exit problem between the period-1 attractor and the period-3 saddle in the simplified system given by Eqs. (10) and (12).

In the following context, the derivation of MFPT is just sketched at first for the completeness of this paper. In addition, since the model here is about a system with much higher dimensions and more complicated dynamical structures, the results obtained by Z. Schuss and his co-workers are not concise enough to deal with the problem directly here, thus some approximation method is needed to simplify the formula.

Suppose that $\tau_\epsilon(\mathbf{x})$ is the exit time of the trajectory which starts at the point $\mathbf{x} \in \mathrm{D}$ and reaches the boundary $\partial\mathrm{D}$ for the first time. The Pontryagin equation which $\tau_\epsilon(\mathbf{x})$ needs to satisfy is given as

$$\begin{cases} \overline{L}\tau_\epsilon(\mathbf{x}) = -1, & \mathbf{x} \in \mathrm{D}, \\ \tau_\epsilon(\mathbf{x}) = 0, & \mathbf{x} \in \partial\mathrm{D}, \end{cases} \tag{42}$$

where D is the domain within a four-dimensional space, then ∂D is a three-dimensional hypersurface. The solution to Eq. (42) is assumed as

$$\tau_\epsilon(\mathbf{x}) = T_0 \tau_q(\mathbf{x}), \tag{43}$$

where $\tau_q(\mathbf{x})$ is the boundary layer function and T_0 is a constant, which, according to the second interpretation in [Naeh *et al.*, 1990], is formulated by

$$T_0 = \frac{\displaystyle\int_{\mathrm{D}} p(\mathbf{x}) \mathrm{d}x_1 \mathrm{d}x_2 \mathrm{d}x_3 \mathrm{d}x_4}{\displaystyle\int_{\partial\mathrm{D}} \mathbf{J}(\mathbf{x}) \cdot \mathbf{v}(\mathbf{x}) \mathrm{d}s_1 \mathrm{d}s_2 \mathrm{d}s_3} \tag{44}$$

where $\mathbf{J}$ is the stationary probability current density and the components J_i of which are defined as

$$J_i = b_i p(\mathbf{x}) - \frac{\epsilon}{2} \sum_{j=1}^{4} \partial_j (a_{ij} p(\mathbf{x})) \tag{45}$$

and $\mathbf{v}$ is the outer normal vector of the boundary ∂D, each s_i for $i = 1, \ldots, 3$ is the variable of integration along the boundary ∂D.

Before the calculation for Eq. (44), the domain D and its boundary ∂D are needed to be defined specifically [Roy, 1997b; Roy & Nauman, 1995; Roy, 1994b, 1997a, 1995], i.e.

$$\begin{cases} \mathrm{D} = \{\mathbf{x} \,|\, \psi(\mathbf{x}) \le \hat{\psi}\}, \\ \partial\mathrm{D} = \{\mathbf{x} \,|\, \psi(\mathbf{x}) = \hat{\psi}\}, \end{cases} \tag{46}$$

where $\hat{\psi}$ is a constant determined artificially. The condition Eq. (35) of noncharacteristic boundaries is satisfied by an appropriate choice of $\hat{\psi}$. And under the definition of Eq. (46), the outer normal vector of ∂D is derived, i.e.

$$\mathbf{v} = \frac{[p_1 \quad p_2 \quad p_3 \quad p_4]}{\sqrt{\displaystyle\sum_{i=1}^{4} p_i^2}}. \tag{47}$$

Int. J. Bifurcation Chaos 2017.27. Downloaded from www.worldscientific.com
by HONG KONG POLYTECHNIC UNIVERSITY on 04/20/19. Re-use and distribution is strictly not permitted, except for Open Access articles.

By substituting Eqs. (19), (45), (47) and (41) into Eq. (44), the formula of MFPT is derived:

$$T_0 = \frac{\displaystyle\int_D w(\mathbf{x}) \exp\left(-\frac{\psi(\mathbf{x})}{\epsilon}\right) q(\mathbf{x}) \mathrm{d}x_1 \mathrm{d}x_2 \mathrm{d}x_3 \mathrm{d}x_4}{\displaystyle\int_{\partial D} \left[w(\mathbf{x}) \sum_{i,j=1}^{4} a_{ij} p_i(\mathbf{x}) p_j(\mathbf{x}) \exp\left(-\frac{\psi(\mathbf{x}^b)}{\epsilon}\right)\right] \Bigg/ \left(2\sqrt{\sum_{i=1}^{4} p_i^2(\mathbf{x})}\right) \mathrm{d}s_1 \mathrm{d}s_2 \mathrm{d}s_3}. \tag{48}$$

However, due to the high-dimensional integral in Eq. (48), this result is hardly available for a direct calculation, then the Laplace approximation and the condition given in Eq. (20) are applied to reduce the complexity of the calculation, which leads to

$$T_0 = \frac{2\sqrt{2\pi\epsilon}\sqrt{\displaystyle\sum_{i=1}^{4} p_i^2(\mathbf{x}^b)} \exp\left(\frac{\psi(\mathbf{x}^b)}{\epsilon}\right) \sqrt{\det(\mathbf{H}(\mathbf{x}^b))}}{\sqrt{\det(\mathbf{H}(\mathbf{x}^*))} w(\mathbf{x}^b) \displaystyle\sum_{i,j=1}^{4} a_{ij} p_i(\mathbf{x}^b) p_j(\mathbf{x}^b)}, \tag{49}$$

where the matrix $\mathbf{H}$ is the Hessian matrix of $\psi(\mathbf{x})$ and $\mathbf{x}^b$ is the point where the ray and the boundary intersect. In comparison with Eq. (48), Eq. (49) is simpler, and furthermore, for the estimation of MFPT, there is no need to calculate a family of rays that cover the domain D, just a calculation for one ray which connects the initial point $\mathbf{x}_0$ that is given in Eq. (32) and the point of $\mathbf{x}^b$ is enough.

With Eq. (49), the MFPT under a set of parameters mentioned above is estimated and compares with the numerical result simulated by the Monte Carlo method. However during the analysis process, the authors have to face a new problem of which the matrix $\mathbf{C}^{\mathrm{T}}\mathbf{C}$ that is defined in Eq. (31) is ill-conditioned and directly leads to its inaccurate inverse matrix. The condition number is used to characterize how ill-conditioned the matrix $\mathbf{C}^{\mathrm{T}}\mathbf{C}$ is. Figure 7(a) shows the variation of the condition number of the matrix $\mathbf{C}^{\mathrm{T}}\mathbf{C}$ versus the coordinate s along one ray.

In Fig. 7(a), the ill-conditioned degree is very serious. For example, if $s = 34.25$, the condition number of $\mathbf{C}^{\mathrm{T}}\mathbf{C}$ is 2.1358×10^9. Under this condition, if there are ten linear equations, the coefficient matrix of full rank can be selected from the 16 linear equations in Eq. (30), there are 2304 choices in which the maximum condition number of the coefficient matrix is 1.18×10^8, and the minimum one is 4.41×10^4. There is no doubt that the problem of ill-conditioned matrix may lead to the incorrect solution or no solution of $w(\mathbf{x})$ to Eq. (19). And Fig. 7(b) shows how the ill-conditioned matrix influences the prefactor function $w(\mathbf{x})$ and the function $w(\mathbf{x})$ is $O(1)$ before the matrix gets ill-conditioned. It is noted that these numerical complexities are caused by the nonsmoothness effect of the piecewise linear function and cannot be avoided by choosing

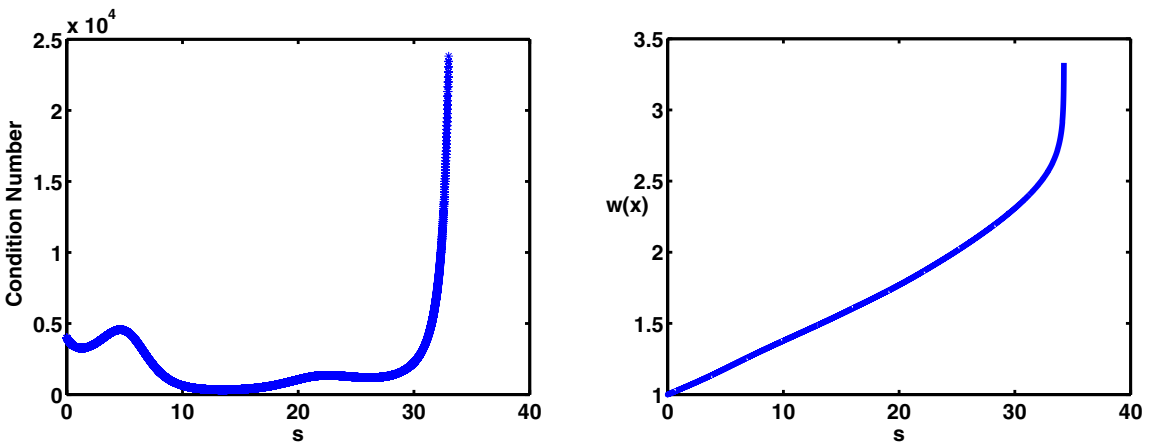

(a) (b)

Fig. 7. (a) The condition number of the matrix $\mathbf{C}^{\mathrm{T}}\mathbf{C}$ in Eq. (31) during the process of calculation for one ray. In order to display the variation of the condition number, the peak value of the condition number does not appear in this figure and (b) the function $w(\mathbf{x})$ in Eq. (19) during the same process for the same ray.

Int. J. Bifurcation Chaos 2017.27. Downloaded from www.worldscientific.com
by HONG KONG POLYTECHNIC UNIVERSITY on 04/20/19. Re-use and distribution is strictly not permitted, except for Open Access articles.

a much smaller step size in numerical process [Hu, 1995]. Detailed discussions about these numerical complexities are beyond the scope of this paper, and will be given in the further work. Here, we follow the method used in [Roy, 1996] and [Ludwig, 1975]. Since $w(\mathbf{x})$ is of the order $O(1)$ before the matrix gets ill-conditioned as shown in Fig. 7(b), the term $w(\mathbf{x}^b)$ in Eq. (49) is then ignored without loss of much accuracy. The final solution of MFPT is obtained, i.e.

$$T_0 \approx \frac{2\sqrt{2\pi\epsilon}\sqrt{\sum_{i=1}^{4} p_i^2(\mathbf{x}^b)}\exp\left(\frac{\psi(\mathbf{x}^b)}{\epsilon}\right)\sqrt{\det(\mathbf{H}(\mathbf{x}^b))}}{\sqrt{\det(\mathbf{H}(\mathbf{x}^*))}\sum_{i,j=1}^{4} a_{ij}p_i(\mathbf{x}^b)p_j(\mathbf{x}^b)}. \tag{50}$$

It is remarked that in Eq. (31) the matrix $\mathbf{C}$ is involved in the calculation of the matrix $\mathbf{H}$, so it must be ensured that the matrix $\mathbf{C}$ is not ill-conditioned during the calculation.

As discussed in Sec. 2, the case of $\omega = 0.89$ is selected as the typical one for the estimation of the MFPT. There are two solutions to Eq. (13), one is the period-1 solution, which is under the condition that $a_s = -4.6291$, $b_s = -1.7403$, $c_s = 0.2874$, $d_s = 2.9451e-4$, $e_s = -5.0282e-6$, the other is the period-3 solution, which is under the condition that $a_s = -0.6931$, $b_s = -0.0779$, $c_s = 0.6308$, $d_s = 0.2529$, $e_s = 1.1417$. These results demonstrate that the approximation Eq. (6) gives appropriate expressions of both the subharmonic solution (period-3) and the harmonic solution (period-1), and the dynamical behaviors such as the subharmonic motions and the harmonic ones given by the deterministic version of the averaged system match the ones of the original system.

On the basis of the solutions obtained above and the result given in Eq. (50), domain D is defined via Eq. (46), wherein $\hat{\psi} = 0.00069$ is selected. And the methods used above, like the averaging method and WKB approximation, are valid in the case $\epsilon \to 0$, i.e. $D \to 0$, while the Monte Carlo simulations can be only applied with finite noise intensity D. Thus D^{-1} values in Fig. 8 are chosen to vary between 5000 and 18 000. When D is chosen in this interval, D is very small and of order $O(10^{-5})$, and meanwhile the numerical simulations do not cost too much time. Then the final result of MFPT is estimated and the curve is plotted in Fig. 8,

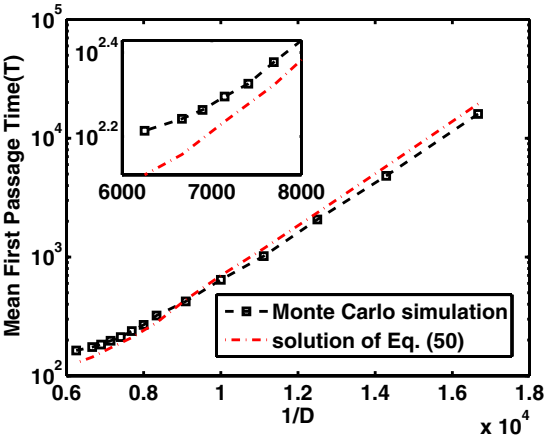

Fig. 8. The MFPT with Eq. (50) is compared with the result simulated by the Monte Carlo method versus D^{-1}. Inset: The details of a part of the main figure when D is large.

which matches the result given by the Monte Carlo simulation. The simulation results are obtained by averaging 10 000 samples at each data point. These two curves are both displayed versus D^{-1} on the semi-logarithmic plot to get a clear observation of the almost linear relationship between the logarithm of MFPT and D^{-1} according to Eq. (50).

As the noise intensity D becomes large, i.e. D^{-1} becomes small, the error between these two results also becomes large as shown in the inset of Fig. 8. This fact is caused by Eq. (50) which is valid in the case $D \to 0$. When the noise intensity D becomes small, i.e. D^{-1} becomes large, one can claim the agreement between these two results. These results demonstrate that the transitions between the attractor and the saddle in simplified system Eq. (10) can be used to analyze the noise-induced chaos, and also demonstrate that Eq. (50) is useful to estimate the phenomenon of noise-induced chaos and the influence of the chaotic saddle in the exit problem quantitatively.

6. Conclusions and Discussions

The phenomenon of noise-induced chaos in a piecewise linear system that is subjected to both Gaussian white noise and harmonic excitation is investigated. This phenomenon depends on the existence of a chaotic saddle around a regular attractor. Noise drives the system to switch between the chaotic saddle and the regular attractor intermittently. So the onset and termination of this phenomenon are partly determined by the deterministic bifurcation which creates and destroys the chaotic

Int. J. Bifurcation Chaos 2017.27. Downloaded from www.worldscientific.com
by HONG KONG POLYTECHNIC UNIVERSITY on 04/20/19. Re-use and distribution is strictly not permitted, except for Open Access articles.

saddle. And we choose the concept of MFPT to measure this phenomenon of noise-induced chaos quantitatively. After the onset of the noise-induced chaos, a tiny noise can induce large displacements from the deterministic stable state and the MFPT is expected to be finite. Compared to regular situations, such a tiny noise could be expected to induce tiny displacements from the deterministic stable state and the MFPT is expected to be infinite.

For the relevant system in the absence of noise, through the numerical GCMD method, a chaotic saddle is first found just around the attractor. It is noted that for the system of structural instability, even a very small noise excitation leads to a transition between the chaotic attractor and a periodic motion [Fig. 1(a)]. Based on an assumption of the approximate expression about the trajectory of the periodic motions, the piecewise linear system is simplified to a four-dimensional Itô system by using stochastic averaging method. Thus for the noise-driven system, the investigation on the phenomenon of noise-induced chaos in the original system is replaced by the one on the phenomenon of transition between a stable attractor and a saddle in the simplified system. Then the formula of MFPT is obtained by using the singular perturbation method and the Laplace approximation. In this process, the effect of boundary layer is considered.

Within the analysis, a serious problem the authors have to face is that an ill-conditioned matrix arises and hinders the calculation of MFPT. Since the condition number of this matrix is too large to obtain the accurate inverse matrix, one more approximation is applied to simplify the final form of MFPT. The comparison between the final result and the numerical simulation confirms that the approximation method is available to characterize the phenomenon of noise-induced chaos quantitatively, and the transitions between the attractor and the saddle in simplified system can be used to analyze the noise-induced chaos.

Although Eq. (1) is a general piecewise linear system, we have noticed that in other types of nonlinear systems, not all noise-induced chaos can be approximated to transitions between an attractor and a saddle. If this approximation fails, the analytical procedure cannot work. Besides this, when the intensity of noise exceeds some level, noise-induced chaos disappears in this piecewise linear system. To characterize both the onset and termination of noise-induced chaos, more concepts and techniques of random dynamics should be involved, like random attractors and the stochastic bifurcation. To devise a more general method to study the onset and termination of noise-induced chaos phenomenon in more complicated nonlinear systems with multiple stable periodic attractors will be the future direction of our works.

Acknowledgments

This work was supported by the National Natural Science Foundation of China (No. 11472126), the Research Fund of State Key Laboratory of Mechanics and Control of Mechanical Structures (Nanjing University of Aeronautics and Astronautics) (Grant No. MCMS-0116G01), and a Project Funded by the Priority Academic Program Development of Jiangsu Higher Education Institutions (PAPD).

References

Armbruster, D., Stone, E. & Kirk, V. [2003] "Noisy heteroclinic networks," *Chaos* **13**, 71–79.

Aubry, N., Holmes, P., Lumley, J. L. & Stone, E. [1988] "The dynamics of coherent structures in the wall region of a turbulent boundary layer," *J. Fluid Mech.* **192**, 115–173.

Billings, L. & Schwartz, I. B. [2002] "Exciting chaos with noise: Unexpected dynamics in epidemic outbreaks," *J. Math. Biol.* **44**, 31–48.

Bobrovsky, B. Z. & Schuss, Z. [1982] "A singular perturbation method for the computation of the mean first passage time in a nonlinear filter," *SIAM J. Appl. Math.* **42**, 174–187.

Chen, L. C., Deng, M. L. & Zhu, W. Q. [2009] "First passage failure of quasi integrable-Hamiltonian systems under combined harmonic and white noise excitations," *Acta Mech.* **206**, 133–148.

Chen, L. C. & Zhu, W. Q. [2010] "First passage failure of quasi-partial integrable generalized Hamiltonian systems," *Int. J. Non-Lin. Mech.* **45**, 56–62.

Dellnitz, M., Froyland, G. & Junge, O. [2001] "The algorithms behind GAIO-set oriented numerical methods for dynamical systems," *Ergodic Theory, Analysis, and Efficient Simulation of Dynamical Systems* (Springer), pp. 145–174.

Dtchetgnia Djeundam, S. R., Yamapi, R., Kofane, T. C. & Aziz-Alaoui, M. A. [2013] "Deterministic and stochastic bifurcations in the Hindmarsh–Rose neuronal model," *Chaos* **23**, 033125.

Ellner, S. & Turchin, P. [1995] "Chaos in a noisy world: New method and evidence from time series analysis," *Am. Nat.* **145**, 343–375.

Int. J. Bifurcation Chaos 2017.27. Downloaded from www.worldscientific.com
by HONG KONG POLYTECHNIC UNIVERSITY on 04/20/19. Re-use and distribution is strictly not permitted, except for Open Access articles.

Freidlin, M. I. & Wentzell, A. D. [2012] *Random Perturbations of Dynamical Systems*, 3rd edition (Springer).

Guckenheimer, J. & Holmes, P. [1983] *Nonlinear Oscillations, Dynamical Systems, and Bifurcations of Vector Fields* (Springer-Verlag, NY).

Han, Q., Xu, W. & Yue, X. [2014] "Global bifurcation analysis of a Duffing–Van der Pol oscillator with parametric excitation," *Int. J. Bifurcation and Chaos* **24**, 1450051-1–11.

Han, Q., Xu, W., Yue, X. & Zhang, Y. [2015] "First-passage time statistics in a bistable system subject to Poisson white noise by the generalized cell mapping method," *Commun. Nonlin. Sci. Numer. Simul.* **23**, 220–228.

He, T. & Habib, S. [2013] "Chaos and noise," *Chaos* **23**, 033123.

Hikihara, T., Perkins, E. & Balachandran, B. [2012] "Noise-enhanced response of nonlinear oscillators," *Procedia IUTAM* **5**, 59–68.

Hong, L. & Xu, J. [2003] "Chaotic saddles in Wada basin boundaries and their bifurcations by the generalized cell-mapping digraph (GCMD) method," *Nonlin. Dyn.* **32**, 371–385.

Hong, L. [2010] "A fuzzy crisis in a Duffing–van der Pol system," *Chin. Phys. B* **19**, 1–6.

Hong, L., Zhang, Y. & Jiang, J. [2010] "A hyperchaotic crisis," *Int. J. Bifurcation and Chaos* **20**, 1193–1200.

Hsu, C. S. [1987] *Cell-to-Cell Mapping: A Method of Global Analyis for Nonlinear Systems* (Springer-Verlag, NY).

Hsu, C. S. [1995] "Global analysis of dynamical systems using posets and digraphs," *Int. J. Bifurcation and Chaos* **5**, 1085–1118.

Hu, H. [1995] "Simulation complexities in the dynamics of a continuously piecewise-linear oscillator," *Chaos Solit. Fract.* **5**, 2201–2212.

Hunt, B., Ott, E. & Yorke, J. [1996] "Fractal dimensions of chaotic saddles of dynamical systems," *Phys. Rev. E* **54**, 4819–4823.

Klosek-Dygas, M., Matkowsky, B. J. & Schuss, Z. [1988] "Stochastic stability of nonlinear oscillators," *SIAM J. Appl. Math.* **48**, 1115–1127.

Kong, C., Gao, X. & Liu, X. [2016] "On the global analysis of a piecewise linear system that is excited by a Gaussian white noise," *J. Comput. Nonlin. Dyn.* **11**, 051029-1.

Kraut, S. & Feudel, U. [2002] "Multistability, noise, and attractor hopping: The crucial role of chaotic saddles," *Phys. Rev. E* **66**, 1–4.

Kraut, S. & Feudel, U. [2003a] "Enhancement of noise-induced escape through the existence of a chaotic saddle," *Phys. Rev. E* **67**, 015204.

Kraut, S. & Feudel, U. [2003b] "Noise-induced escape through a chaotic saddle: Lowering of the activation energy," *Physica D* **181**, 222–234.

Lin, K. K. & Young, L.-S. [2008] "Shear-induced chaos," *Nonlinearity* **21**, 899–922.

Ludwig, D. [1975] "Persistence of dynamical systems under random perturbations," *SIAM Rev.* **17**, 605–640.

Naeh, T., Kłosek, M. M., Matkowsky, B. J. & Schuss, Z. [1990] "A direct approach to the exit problem," *SIAM J. Appl. Math.* **50**, 595–627.

Rodrigues, C. S., Grebogi, C. & De Moura, A. P. S. [2010] "Escape from attracting sets in randomly perturbed systems," *Phys. Rev. E* **82**, 1–5.

Roy, R. [1994a] "Averaging method for strongly nonlinear oscillators with periodic excitations," *Int. J. Non-Lin. Mech.* **29**, 737–753.

Roy, R. [1994b] "Noise perturbations of a non-linear system with multiple steady states," *Int. J. Non-Lin. Mech.* **29**, 755–773.

Roy, R. V. [1995] "Noise-induced transitions in weakly-nonlinear oscillators near resonance," *J. Appl. Mech.* **62**, 496–504.

Roy, R. V. & Nauman, E. [1995] "Noise-induced effects on a non-linear oscillator," *J. Sound Vibr.* **183**, 269–295.

Roy, R. [1996] "Probabilistic analysis of a nonlinear pendulum," *Acta Mech.* **115**, 87–101.

Roy, R. [1997a] "Asymptotic analysis of first-passage problems," *Int. J. Non-Lin. Mech.* **32**, 173–186.

Roy, R. V. [1997b] "Global stability analysis of nonlinear dynamical systems," *Uncertainty Modeling in Finite Element, Fatigure and Stability of Systems*, Series on Stability, Vibration and Control of Systems Series B, Vol. 9 (World Scientific), pp. 261–295.

Stone, E. & Armbruster, D. [1999] "Noise and $O(1)$ amplitude effects on heteroclinic cycles," *Chaos* **9**, 499–506.

Tél, T., Lai, Y.-C. & Gruiz, M. [2008] "Noise-induced chaos: A consequence of long deterministic transients," *Int. J. Bifurcation and Chaos* **18**, 509–520.

Young, L.-S. [1986] "Stochastic stability of hyperbolic attractors," *Ergod. Th. Dyn. Syst.* **6**, 311–319.

Yue, X., Xu, W. & Zhang, Y. [2012] "Global bifurcation analysis of Rayleigh–Duffing oscillator through the composite cell coordinate system method," *Nonlin. Dyn.* **69**, 437–457.

Zhou, C. S., Kurths, J., Allaria, E., Boccaletti, S., Meucci, R. & Arecchi, F. T. [2003] "Constructive effects of noise in homoclinic chaotic systems," *Phys. Rev. E* **67**, 066220.